X-ray study of phases and structures in ^{3}He-^{4}He solid solutions

B. A. Fraass* and R. O. Simmons
Physics Department and Materials Research Laboratory, University of Illinois at Urbana-Champaign, 1110 West Green Street, Urbana, Illinois 61801
(Received 5 January 1987)

X-ray diffraction has been used to study structural and thermodynamic aspects of isotopic phase separation in solid mixtures of ^{3}He and ^{4}He. The phase-separation process has been followed in crystals of 51%, 28%, and 12% ^{3}He and melting pressures between 3.0 and 6.1 MPa. The phase-separation temperatures determined in this work on massive crystals are in general agreement with previous work using other techniques. The pressure dependence of T_c, the highest temperature on the coexistence curve, is found to be linear: $dT_c/dP = -34$ mdeg/MPa. The resulting molar volume of mixing is $v^E = -0.54x(1-x)$ cm^3. Deviation from regular solution behavior, reported in the literature, while possible, is not confirmed. The results of these x-ray measurements also yield detailed structural information which modifies previous understanding of the low-temperature, low-pressure phase diagram of helium isotopic mixtures.

I. INTRODUCTION

Solid helium is a remarkable subject for study from both theoretical and experimental viewpoints. The basis for this interest is that the vibrational energy is comparable to its potential energy.[1] One manifestation of this relatively weak binding and small atomic mass is that the rms deviation $\langle u^2\rangle^{1/2}$ of atoms from their equilibrium atomic sites is very large,[2] compared to the nearest-neighbor distance R. The nonlocalization of the atom from its lattice site has at least three results: (1) neighboring atoms are encountered at distances on the order of their hard-core radii, (2) the "small" parameter of classical lattice dynamics, $\langle u^2\rangle^{1/2}/R$, is not small, and (3) neighboring atoms may tunnel and exchange lattice sites.[3,4]

Addition of ^{3}He to ^{4}He produces enlargement of the PVT domain having bcc structure. Melting curves and bcc-hcp transformation temperatures have been studied by means of ultrasonic,[5] NMR,[6,7] thermal conductivity,[8] and pressure[9,10] measurements. While consistency of the various melting measurements is fairly good, determination of the bcc-hcp boundary seems less satisfactory.[11] Figure 1 shows the situation, schematically, for a 5% addition to ^{3}He ($x=0.05$). Further additions of ^{3}He provide an extended domain of bcc phase from melting down to low temperatures.

The purpose of the present work is to study structural aspects of isotopic phase separation in the bcc phase of the concentrated He solid mixtures. Such separation, into ^{3}He-rich and ^{4}He-rich components below the phase-separation temperature (T_{PS}), was first reported from calorimetry in 1962 by Edwards and co-workers,[12,13] who found that $T_{PS}=0.38$ K for $x=0.5$ and $P=3.63$ MPa. Later experimental investigators used pressure[9,10,14–16] and thermal conductivity[17] as a signature of separation. In solid helium the atomic tunneling and exchange processes allow macroscopic separation into two components on a reasonable time scale for experimental study.

Here, we report results using x-ray diffraction techniques, which unlike the earlier methods, can yield information about the individual ^{3}He-rich and ^{4}He-rich phases,[18] as well as about the low-temperature phase diagram. The crystallographic situation is, for the most part, simplified at the pressures we used because the original homogeneous mixture and both daughter separated phases are largely bcc. Although the latter phases develop substantially different lattice parameters they appear with generally the same orientation. Transparency of the solid helium samples to x rays allows these phenomena to be studied in the bulk. The present work was carried out over a larger pressure range than previous studies and allows determination of T_{PS} and its pressure derivative.

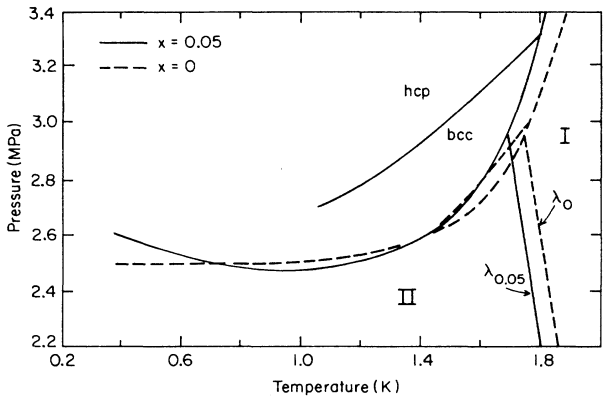

FIG. 1. Schematic low pressure P-T phase diagrams for pure ^{4}He and for ^{4}He with 5% ^{3}He concentration ($x=0$ and 0.05, respectively). The dashed lines show the pure ^{4}He melting line, λ line between normal (I) and superfluid (II), and bcc-hcp boundary. The solid lines are for $x=0.05$. Note that the bcc phase increases in extent in the mixture, and that the melting curve minimum is made more prominent by the addition of ^{3}He.

II. THERMODYNAMICS OF MIXTURES

A. Phase separation (miscibility gap)

The free energy of mixing, f^M, of two pure substances is defined as

$$f^M = f(V,T,x) - xf(V,T,x=1) - (1-x)f(V,T,x=0) , \tag{1}$$

where x is the fraction of one of them.[19] The volume of mixing is

$$v^M = v - xv(x=1) - (1-x)v(x=0) , \tag{2}$$

and the entropy s and pressure p of mixing are given by

$$s^M = -(\partial f^M/\partial V)_V \tag{3}$$

and

$$p^M = -(\partial f^M/\partial V)_T . \tag{4}$$

Regarding the molar total energy of the crystal as composed of various interatomic interactions of the pairs of atoms, isotopes 3 and 4, one has for the molar total energy

$$u = \tfrac{1}{2}zx^2 e_{33} + \tfrac{1}{2}z(1-x)^2 e_{44} + zx(1-x)e_{34} \tag{5}$$

($z=8$ for bcc). From this one obtains

$$u^M = u - xu(x=1) - (1-x)u(x=0) = zx(1-x)w , \tag{6}$$

where the interaction energy w is

$$w = e_{34} - \tfrac{1}{2}(e_{33}+e_{44}) . \tag{7}$$

For a regular solution $s^M = s^M(\text{ideal})$ but $w \neq 0$. In this case

$$\begin{aligned} f^M &= u^M - Ts^M \\ &= x(1-x)w + T[x\ln(x) + (1-x)\ln(1-x)] \end{aligned} \tag{8}$$

and the temperature of critical mixing, T_c, determined by the condition that $\partial f^M/\partial x = \partial^2 f^M/\partial x^2 = 0$, is

$$T_c = w/2 . \tag{9}$$

In general, T_c is a function of volume. The shape of the phase-separation curve for a regular solution is

$$T_{PS} = 4T_c(x-\tfrac{1}{2})/\ln[x/(1-x)] . \tag{10}$$

It is usual to describe a real solution in terms of excess properties, i.e., the values compared to the properties of a hypothetical ideal solution. In a regular solution, the excess energy u^E, excess volume v^E, and excess pressure p^E are identical to the mixing values, u^M, v^M, and p^M, respectively. One finds from differentiation of the Helmholz energy f that

$$\begin{aligned} f^E &= -x(1-x)(\partial w/\partial V)_T \\ &= -x(1-x)2(dT_c/dV) , \end{aligned} \tag{11}$$

that is, the excess pressure is determined by the volume dependence of T_c and hence of w. An analogous differentiation of the Gibbs energy gives

$$v^E = x(1-x)2(dT_c/dP) . \tag{12}$$

B. Particulars of the He isotope mixture phase diagram

Mullin[20] uses a model generalized from Nosanow theory[21] to calculate for solid solutions of the helium isotopes

$$v^E = cx(1-x) , \quad c = -0.4 \text{ cm}^3/\text{mol} . \tag{13}$$

He notes that, owing to vibrational zero-point effects, the equilibrium volume of pure ^{3}He is larger than that of pure ^{4}He at an equal applied pressure, and from his model there is a small deviation from regular solution behavior,

$$g^E(x,P) = x(1-x)[w_0(P) + w_1(P)x] . \tag{14}$$

At 3.63 MPa (the pressure of the original experiments),[13] he finds $w_0 \sim 1.0$ K and $w_1 \sim -0.1$ K. The low-x part of the T_{PS} versus x curve then is expected to be higher than predicted by the symmetric relation, Eq. (10). Mullin's calculation also gives $T_c \sim 0.47$ K, compared to the experimental value of 0.38 K at this pressure, and it predicts that $dT_c/dP \sim -24$ mdeg/MPa.

At low pressures, near those needed to solidify the helium isotopes, there are other complications in the T_{PS} versus x phase diagram of the mixtures. On the ^{4}He-rich side (small x), there is a mixed bcc-hcp region. From the Gibbs phase rule, this mixed phase must terminate at a univariant where it meets the separation curve, but there is no thermodynamic constraint as to where this occurs. On the ^{3}He-rich side (large x), owing to the pronounced minimum in the melting curve, there is a ^{3}He-rich liquid-bcc mixed region, which must also terminate at a univariant. Again, there is no thermodynamic constraint as to where this lies; it may be at a temperature above or below that of the univariant mentioned previously. The inferences of Tedrow and Lee[10] placed it below; we have determined it to be above (Sec. V B).

C. Kinetics and microscopics of He phase separation

The time evolution of phase separation has been analyzed for dilute ^{4}He in ^{3}He (x very near unity) in terms of nucleation and growth by Uwaha,[22] who treats the pressure-change data of Henricksen and co-workers.[15] Uwaha's model which treats atomic exchange processes is consistent with the dependence upon molar volume that they found, namely an increase in the characteristic time from about 3×10^2 s at 24.18 cm^3 to about 5×10^4 s at 21.26 cm^3. For an x-ray experimental technique on initially single crystals of the homogeneous mixture, some hysteresis and microstructural anomalies would not be surprising for times less than these.

It is expected that the early stages of decomposition in bcc helium isotope mixtures involve a continuous process in which the new phases start out crystallographically coherent with one another. A general review of such processes is given by Cahn.[23] In helium isotope mixtures, however, these new phases develop lattice parameters differing by several percent at lower temperatures (Sec.

IV). Coherency is doubtful in such circumstances, so the remixing process upon heating may have complications.

Decomposition in solid helium isotope mixtures has been observed optically with the technique of real-time holographic interferometry.[24] Fine-grained domains, rather randomly connected and with edges apparently predominantly aligned in a few directions, are seen.[25] The scale of the domains changes with time, but the size of the smaller visible ones is consistent with the absence of x-ray crystallite size broadening in the current work (see Sec. V B 1).

III. EXPERIMENTAL TECHNIQUES

Successful x-ray diffraction study of phase-separation phenomena depends upon experimental apparatus which covers a sufficient portion of reciprocal space. In the case of solid helium, for which the form factor restricts study with conventional x-ray sources to essentially forward scattering, one depends upon there being somewhat predictable orientational relationships between the parent homogeneous phase and the daughter phases which appear during the phase-separation process. For this reason, we based the present exploration upon preparation of single-crystal specimens at high temperatures and upon controlled temperature cycling of these samples held in precise relation to a special orientable diffractometer having a position-sensitive detector (PSD). Descriptions of the cryostat,[26] x-ray diffractometer,[27] and sample preparation and analysis procedures[28] are given in the cited references. Reference 28, a parallel study of higher-temperature defects in concentrated isotope mixtures, contains specifics about the samples of the present study.

Available for examination were the size of the x-rayed grain of the sample, its orientation, mosaic spread, lattice parameter (to 300 ppm uncertainty), changes in the lattice parameter (in favorable cases, to 50 ppm uncertainty), and the orientational relation of the daughter phases (in favorable cases). We used Cu $K\alpha$ radiation to examine (110)-type reflections. In all cases the samples were held under pressure at essentially constant macroscopic volume during the entire sequence of measurements reported here. Table I shows that measured lattice parameters of the parent bcc mixed crystals used in the present study. Because a number of these showed apparently large defect content,[28] a corrected molar volume V_0 is also given in Table I when that is possible. Shown also are the molar volumes, V_m, calculated from the PVT measurements of Grilly,[29] using the formula

$$V(x,P)=xV_{^3\mathrm{He}}(P)+(1-x)V_{^4\mathrm{He}}(P)+x(1-x)c \ , \quad (15)$$

where $V_{^3\mathrm{He}}$ and $V_{^4\mathrm{He}}$ are the measured molar volumes of pure ^{3}He and ^{4}He, respectively, at pressure P, and c is

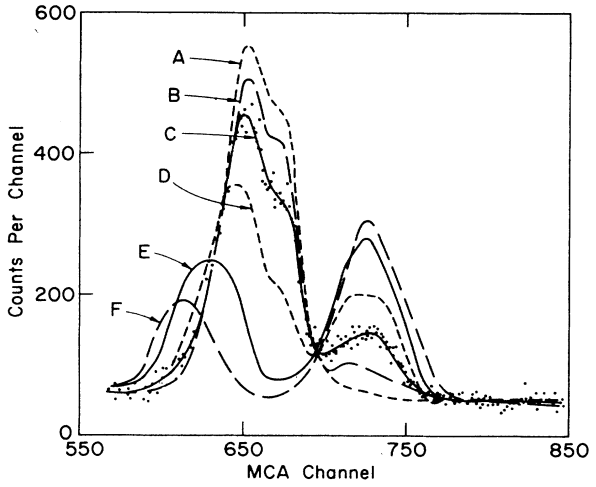

FIG. 2. Bragg (MCA) peak during phase separation of sample no. 26. One degree of arc corresponds to 101.3 channels on the PSD. The evolution of the two separate peaks (which were seen in samples nos. 26, 27, and 28) is clearly visible. For clarity, only one set of raw data is shown (curve *C*), as an example of the method used to determine the other curves. The temperatures at which the successive peaks were obtained are: (*A*) 393 mK; (*B*) 387 mK; (*C*) 381 mK; (*D*) 377 mK; (*E*) 370 mK; (*F*) 359 mK. T_{PS} assigned to sample no. 26 is 388±6 mK.

TABLE I. Lattice parameters and other properties of the bcc mixed ^{3}He-^{4}He samples used. Listed are the ^{3}He concentration (x), melting temperature (T_m), melting pressure (P_m), lattice parameter (a), and the temperature at which it was measured (T_a). Finally, values for the molar volume at the temperature low compared to thermal vacancy effects but above the phase separation temperature (V_0) and for the molar volume V_m calculated from Eq. (15) with data from Ref. 29. The estimated uncertainty in a is 300 ppm, in P_m is 8 kPa, and in the temperatures less than 0.5%. The estimated uncertainty in V_0 is 900 ppm, which corresponds to 0.02 cm^3/mol, and that in V_m is about 0.5%, or 0.1 cm^3/mol. The estimated uncertainty in T_{PS} upon cooling is given in each case.

Sample no.	x (%)	T_m (K)	P_m (MPa)	a (Å)	T_a (K)	V_0 (cm^3)	V_m (cm^3)	T_{PS} (mK)
22	51	2.01	6.178	4.1040	1.893			
23	51	1.99	6.178	4.1109	1.823	20.945	20.43	299±4
				4.1121	1.052			
24	51	1.22	3.220	4.2290	1.089	23.443	22.44	399±6
25	51	1.35	3.565	4.2031	1.246			
26	51	1.33	3.565	4.2013	1.284	23.306	22.12	388±6
27	28	1.87	4.681	4.1264	1.700	21.478	20.54	330±3
28	28	1.58	3.475	4.1739	1.352	22.327	21.35	367±6
29	12	1.701	3.240	4.1291	1.566	21.246	20.95	267±9
				4.1279	1.562			
30	12	1.656	3.041	4.1407	1.381	21.469	21.10	267±3

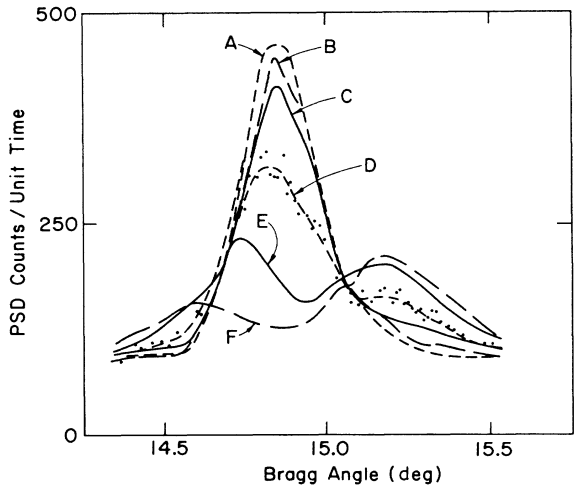

FIG. 3. Mosaic (SCA) peak during phase separation of sample no. 26. The degeneration of mosaic structure of the sample as it phase separated is shown here as a function of temperature. The total number of counts into the PSD per unit time is plotted vs Bragg angle. For clarity, only one set of raw data is shown (curve *D*), as an example of the method used to determine the other curves. The temperatures are the same as those of Fig. 2.

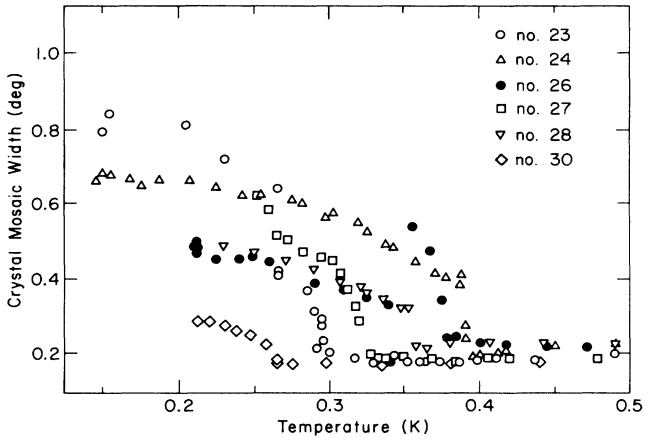

FIG. 4. Crystal mosaic (SCA) width vs temperature for six samples near phase separation. Identification of the various symbols is given in the figure.

Mullin's calculated value [Eq. (13)]. There is apparent disagreement between the deduced molar volumes V_0 and V_m. These differences, although not understood, do not significantly affect the current results on phase separation.

The nature of the PSD data obtainable from a sample undergoing phase separation is shown in Figs. 2 and 3. The two types of x-ray scans, MCA and SCA, are described more completely in Ref. 27. In both types the PSD and x-ray source are fixed with respect to one another and in effect the sample is rotated through the Bragg condition. In the SCA scan the total counts are accumulated in the PSD; this reflects the mosaic structure of the sample. The MCA scan, on the other hand, measures the Bragg angle independently of the mosaic structure of the crystal.

IV. EXPERIMENTAL DATA

A. Summary of results

The phase separation temperature (T_{PS}) found for each concentration x and each pressure is listed in Table I. These values of T_{PS} were obtained in two different ways. The most obvious method was simply to watch the x-ray MCA and SCA peak shapes as the crystal was cooled. There is a clearly recognizable change beginning at T_{PS}. These signatures are shown in Figs. 2 and 3 for sample no. 26. The second method was equating T_{PS} to the temperature at which the lattice parameter versus temperature went through an inflection point. This is similar to the method of Panczyk and co-workers[14] in their strain gauge study of phase separation. The first method is more definite, because the inflection point method is sensitive to the details of the behavior at T_{PS}; this behavior is not always simple.

A quantitative measure of the peak shape changes which are the result of phase separation is the (SCA) width of the crystal mosaic (Fig. 3). These widths, for six different crystals, are shown in Fig. 4.

B. Some details of data

Data taken on sample no. 23 as it was cooled, and then warmed back through T_{PS}, are shown in Fig. 5, taken from MCA data only, since the crystal mosaic broadened considerably below T_{PS}. There is a pronounced dip in the lattice parameter, a, before phase separation; but a rises quickly as soon as the temperature gets below T_{PS}. Although the sample was 49% ^{4}He, only the Bragg peak of the ^{3}He-rich phase was usable. Upon warming, lattice parameter changes were different than when cooling. This

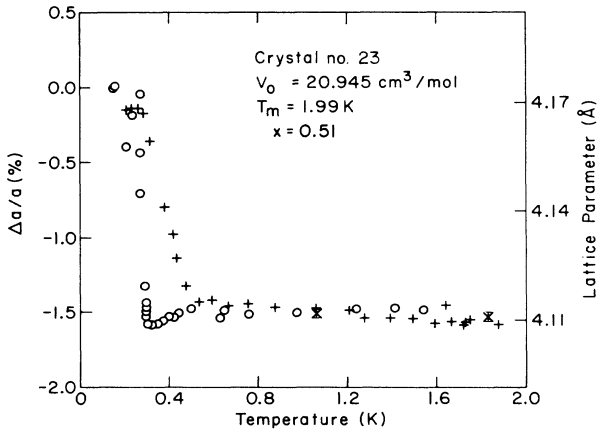

FIG. 5. Crystal sample no. 23 changes in lattice parameter on cooling (circles) and warming (pluses). The lattice parameter values of Table I are shown by ×'s; in the absence of measurable thermal vacancy generation in the temperature range shown above T_{PS}, the lattice parameter is essentially unchanging for the sample contained at constant macroscopic volume. $\Delta a/a$ is arbitrarily referenced to the lowest temperature.

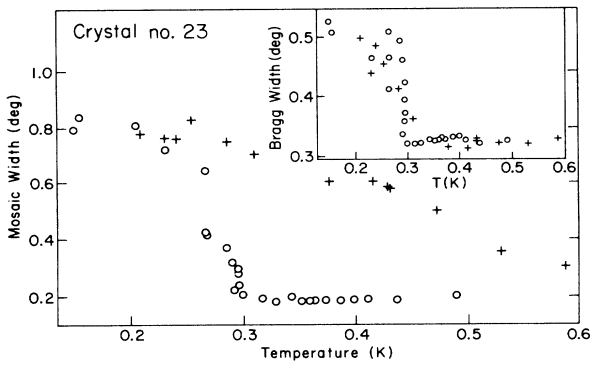

FIG. 6. Crystal sample no. 23 peak widths near T_{PS}. The crystal mosaic which develops upon phase separation is very sluggish to recover upon warming. By contrast, the inset shows that the Bragg peak recovers reversibly for warming at the same rate. Circles denote cooling data; pluses denote warming data.

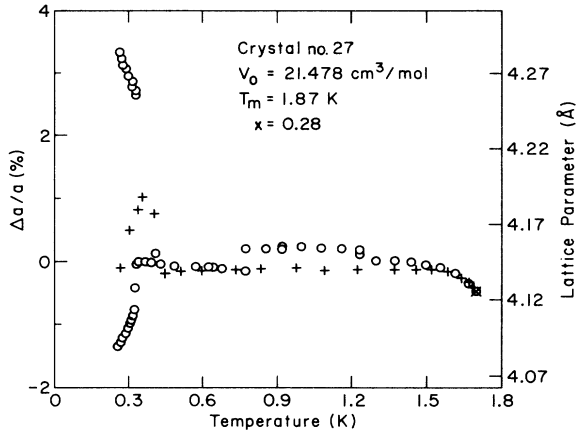

FIG. 8. Crystal sample no. 27 changes in lattice parameter on cooling (circles) and on warming (pluses); lattice parameter (×).

was not time-dependent behavior. This difference between cooling and warming is seen also in Fig. 6, which shows the peak widths in more detail. The Bragg (MCA) width shows no hysteresis. On the other hand, the mosaic (SCA) width upon warming did not decrease to its pre-phase-separation width until after sample no. 23 was warmed very far above T_{PS}.

For sample no. 24 an absolute lattice parameter measurement (x) and all lattice parameters taken upon cooling and warming are shown in Fig. 7. The gap in the cooling data at about 0.37 K is due to a 9-h anneal. A 17-h anneal occurred between the last cooling run point and the lowest temperature point, during which the lattice parameter a increased somewhat. As warming was begun, a increased about 5%; qualitative extrapolation of the cooling curve and the warming curve to T_m shows the two curves apparently meet there.

A slightly higher pressure was used to prepare sample no. 26 than sample no. 24, and their cooling characteristics were similar, down to T_{PS}. Below this temperature, their characteristics differed; sample no. 26 showed two distinct peaks (Figs. 2 and 3, MCA and SCA scans, respectively). This sample sat at 0.35 K for 7 h after separation, after which only the smaller a (^{4}He-rich) peak was left, with its lattice parameter essentially unchanged, but the mosaic width returned near its pre-phase-separation value (see Fig. 4). As sample no. 26 was cooled, the mosaic width again increased. After 10 h at 0.22 K, no peaks were visible. Warming brought back a usable Bragg (MCA) peak, but the mosaic width was spread about 5°.

Both cooling and warming data are shown for sample no. 27 in Fig. 8. At higher temperatures we attribute the disagreements to transition from bcc to a mixed bcc-hcp phase. The decrease in a at 0.77 K came after an 11-h anneal. Below T_{PS} two peaks were visible, but after cooling to 0.255 both appeared to be disappearing, so the sample was warmed. The warming data shown below T_{PS} are not from either of the peaks seen on cooling, but are from the centroid of the two peaks as they coalesced. After warming to 0.9 K and annealing for 9 h, the quality and

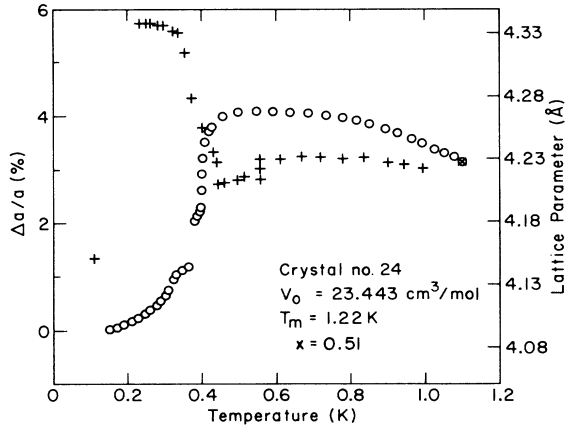

FIG. 7. Crystal sample no. 24 changes in lattice parameter. Symbols are lattice parameter (×), cooling (circle), warming (pluses). Zero for $\Delta a/a$ is arbitrary.

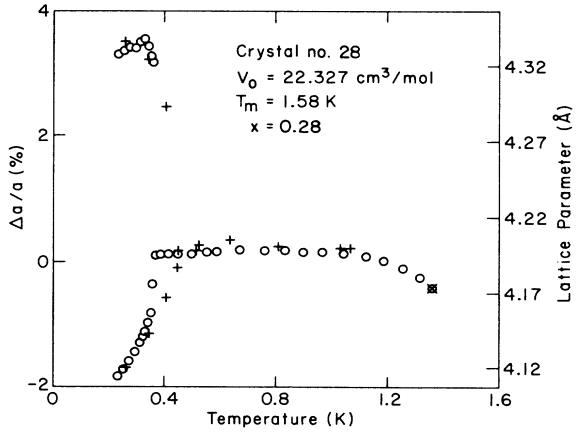

FIG. 9. Crystal sample no. 28 changes in lattice parameter on cooling (circles) and on warming (pluses). The lattice-parameter value is the ×, with its 300 ppm uncertainty barely visible. Note the lattice-parameter compression of the ^{3}He-rich phase, beginning at a distinct temperature (~328 mK), below T_{PS}. For discussion see text Sec. V B.

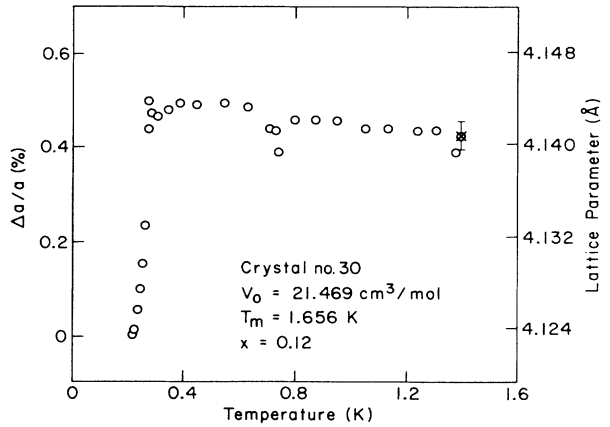

FIG. 10. Crystal sample no. 30 changes in lattice parameter. All the data were obtained on cooling after one absolute lattice-parameter measurement (×). Here the 300 ppm uncertainty is visible. Sample no. 29 also showed lattice-parameter irregularities in the intermediate temperature range, similar to those appearing here.

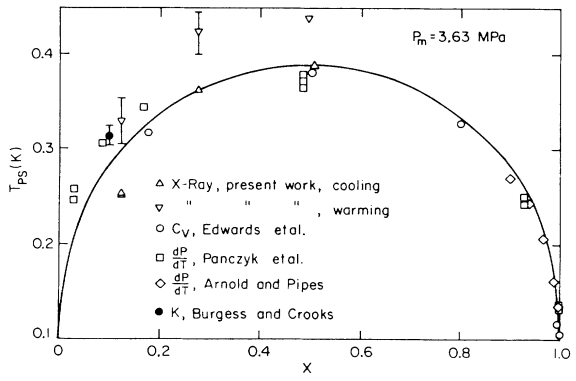

FIG. 11. The phase-separation temperature T_{PS} vs ^{3}He concentration, for different studies (Refs. 13, 14, 16, and 33) and the present x-ray work. An attempt has been made to correct all data to a reference pressure of 3.63 MPa (but see text Sec. V A 3). The curve is regular solution theory, Eq. (10), with T_c determined from present x-ray cooling data (triangles). Illustrative X-ray warming data (inverted triangles) are also shown, with "error bars" simply indicating how widely spaced these individual data points are.

lattice parameter value of the Bragg peak and of the mosaic both returned to their pre-phase-separation values. It seems likely that this was assisted because sample no. 27 did not sit in the separated region for more than 6 h.

Data for sample no. 28 are shown in Fig. 9. The jog in the larger lattice-parameter peak, after separation, was taken as a sign of a phase transition, so this sample, like sample no. 2, was also warmed soon. The agreement of cooling and warming lattice parameters at 0.8 K and above, apparently arises from the sample being below T_{PS} for only 5 h.

Samples nos. 29 and 30 behaved similarly. Sample no. 29 was hardly taken below T_{PS}, so the sample no. 30 data are shown in Fig. 10. The lattice parameter anomaly near 0.74 K occurred after an 11-h anneal.

V. ANALYSIS

A. Isotopic phase separation

1. *Thermodynamic relations*

Most investigators of phase separation in ^{3}He-^{4}He solid solutions have compared their results as a T_{PS} versus x diagram for starting pressures near 3.63 MPa.[13,14,16,20] Therefore, in Fig. 11 phase-separation temperatures are so shown for several sets of data, including the present work. All the data shown are corrected to 3.63 MPa with the pressure dependence of T_{PS} determined in the present work. (Our actual values of T_{PS} are given in Table I.)

To find the pressure dependence of T_{PS}, Eq. (1) was used to obtain a value of T_c for each measured T_{PS}. These T_c's are listed in Table II. dT_c/dP was obtained by a linear fit of these T_c's to the expression $T_c = AP_m + B$, where the melting pressure is used, because the pressure at phase separation is not known. The result is $A = -34$ mdeg/MPa, with a good fit, excluding only sample no. 30 which we classify as showing anomalous behavior. $T_c(P)$ is remarkably linear over the pressure range 3.2 to 6.2 MPa.

Our value of dT_c/dP can be compared to three other determinations. Panczyk and co-workers[14] obtained values which range from -15 to -28 mdeg/MPa, calculated from data over a wide range of x and a range of P from 2.9 to 3.9 MPa. Arnold and Pipes[16] studied concentrations with $x > 0.9$ over the range 3.1 to 4.3 MPa; they

TABLE II. Values of T_c obtained from Eq. (10) with the present results for T_{PS}, Table I. Also shown is the value from Ref. 13. Deviations from a linear fit to the pressure dependence of T_c are also listed, along with the melting pressure P_m. Sample no. 30 is excluded from the fit to obtain the quoted dT_c/dP in Sec. V A 1.

Sample no.	P_m (MPa)	T_c (mK)	Deviation (mK)	Source
23	6.178	299	−1.5	Present work
27	4.681	354	+3.0	Present work
	3.63	378	+9.8	Reference 13
26	3.565	388	−1.3	Present work
28	3.475	394	+1.8	Present work
24	3.220	399	−2.0	Present work
30	3.041	346	−60.8	Present work

report a value -46 mdeg/MPa. Finally, a value has been calculated by Trickey and co-workers[30] from the $x > 0.99$ data of Henriksen and co-workers;[15] they find dT_c/dP approaches zero at pressures above 5 MPa. We believe that determinations of T_c are more likely to be reliable in studies, such as the present one, for concentrations nearer to 50%, where T_c is most nearly equal to T_{PS}.

In regular solution theory, dT_c/dP is related to the excess volume v^E through Eq. (12). Our finding of a constant value of this derivative over the range 3.2 to 6.2 MPa therefore confirms Mullin's prediction[20] that v^E is independent of pressure. Further, numerically in Eq. (13) we find that c is -0.57 cm^3/mol, to be compared to Mullin's value -0.4 cm^3/mol.

2. *Inferences about microcrystalline substructure*

Crude values of the dislocation density, D, in our samples below phase separation can be obtained from the mosaic widths as shown in Fig. 4. An upper limit comes from applying the result of Auleytner[31] that $D < (0.479B/b)^2$, where B is the full width of the crystal mosaic and b the Burgers vector. From our observed widths, Fig. 4, one then finds an upper limit in the range $D \sim 2\times 10^9$ to 1×10^{10} cm^2. A second estimate of D is possible if the structure size t is known, according to Hirsch,[32] whose result is that $D \sim B/3bt$. Burgess and Crooks[33] have estimated $t \sim 0.75$ μm from thermal conductivity data below T_{PS}; this essentially agrees with an estimate by Greenberg and co-workers from NMR work,[17] who find $t \sim 2$ μm. If one puts $t \sim 1$ μm and our mosaic widths B in Hirsch's relation, one obtains $D \sim 4\times 10^8$ to 1×10^9 cm^2. These are to be compared to dislocation densities as low as 10^5 cm^2 which have been estimated in ultrasonic work on isotopically pure, carefully prepared crystalline helium.[34]

3. *Deviations from regular solution behavior*

Generally, the agreement of different experiments with each other and with the regular solution curve of Fig. 11 is good for $x > 0.4$. Any scatter probably can be attributed to differences in temperature scales, to errors in determining T_{PS}, and to uncertainties in correcting to 3.63 MPa (because the melting pressures are not clearly mentioned in the publications). Illustrative points are shown for present warming data; they scatter more, because of the mosaic problems repeatedly noted above.

The apparent disagreements for $x < 0.4$ must be further examined. There are several points to be noted. First, the disagreement of our 12% mixture with the curve is considerable, and not understood. It is interesting that the behavior of the x-ray peak *intensity* was qualitatively different at this concentration. Instead of a degeneration below T_{PS}, the intensity increased by more than 30%. Possibly, the proximity of the hcp-bcc mixed phase accounts for both effects.

Second, the pressures given by Panczyk and co-workers,[14] that were used to correct their data to 3.63 MPa, are pressures immediately above T_{PS}, not P_m. If the large pressure changes thought to accompany thermal defect formation[28] are invoked, then the P_m's of these authors are much higher. This would add a correction as large as 30 mdeg for a 1-MPa pressure difference, and further raise their points in Fig. 11. Third, most of the Panczyk data were taken on warming, which we found to produce slow recovery in the lattice parameter, with an inflection point analogous to the criterion used by Panczyk; our warming data are also shown in Fig. 11. For the warming rates employed, we believe this to produce uncertain results, although they are rather similar to the Panczyk[14] and Burgess and Crooks[33] results. This nonequilibrium type of behavior was noted in NMR work[17] with $x = 1\%$ and 2%, with temperature hysteresis as large as 80 mdeg.

As noted above in Sec. II B, Mullin[20] predicts an asymmetric T_{PS} versus x curve, one which is higher for low x. Because of the uncertainties described above, we cannot regard either our results or those of Panczyk and co-workers[14] as confirming this prediction. We believe more work on this point is needed.[35]

An ingenious analysis applicable to our coexisting daughter-phase lattice parameter data, for which the sample cell in which phase separation occurs has a fixed volume and the numbers of ^{3}He and ^{4}He atoms are conserved, has been devised by Uwaha and Baym.[36] From their analysis of such data (limited to sample no. 27), they conclude that the form of the mixing free energy, Eq. (14), has $w_0 \sim 0.80$ K and $w_1 \sim -0.2$ K. Compared to the values of Mullin (Sec. II B), this conclusion indicates somewhat more asymmetry to the phase-separation curve.

B. Phase-diagram speculations

Our x-ray data obtained below T_{PS} on the individual daughter phases can be analyzed to provide additional information. The T_{PS} curve (Fig. 11) determines the concentration of both the ^{3}He-rich and ^{4}He-rich components of the mixture at each particular temperature. The molar volume of each component (calculated from the observed lattice parameter) can then be plotted against the concentration of that component (inferred from the T_{PS} versus x curve and the temperature of the x-ray data). Therefore, from the x-ray data on a single parent mixture, one can obtain the molar volume of each crystalline daughter everywhere along the concentration axis. If the pressure is known, these measurements yield P, V, T, and phase information for both daughter mixtures at lower temperatures.

The following discussion is for two purposes: to describe the present data qualitatively, and to demonstrate the promise of this technique for obtaining phase diagram information near the region of decomposition. Since the present data are the first of their kind, and exploratory in character, we note several cautions. Our pressures at phase separation are unknown; they can be different from the respective measured melting pressures because there are significant thermal vacancy concentrations in the parent crystals. Second, not all the present data may represent equilibrium conditions. Third, for this discussion we use daughter coexistence concentrations from Eq. (10), with the T_c value from Table II. This assumption of a symmetrical phase-separation curve is not strictly

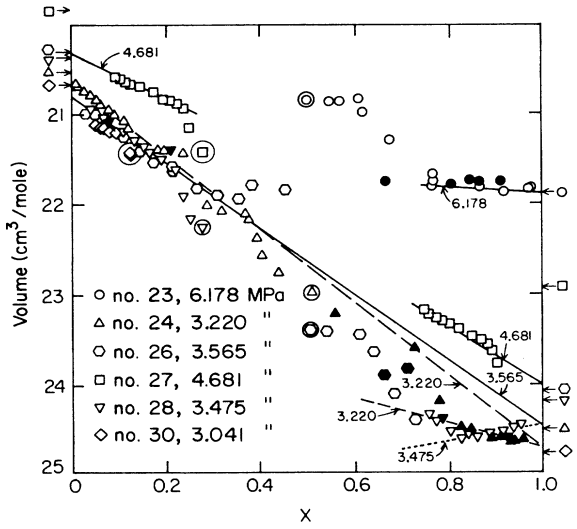

FIG. 12. Molar volumes of the respective daughter phases vs inferred ^{3}He concentration for the various samples below the phase-separation temperature. The values given for the various fitted lines are the respective melting pressures in MPa (see text).

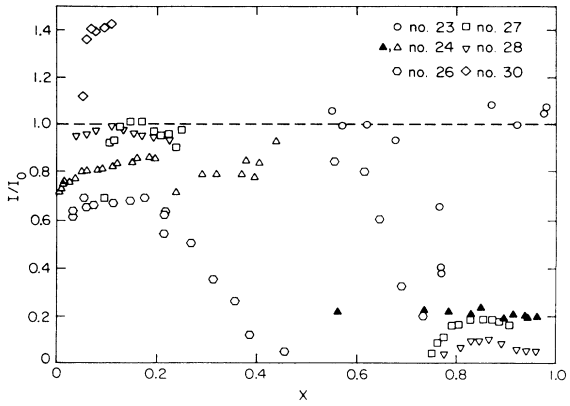

FIG. 13. Relative Bragg peak intensity versus ^{3}He concentration x, calculated as described in Sec. V B. I_0 is the total intensity immediately above T_{PS}. All data are for cooling, except the solid triangles shown for warming of sample no. 24.

satisfied, especially at low temperatures, where there are univariant lines caused by the meeting of a mixed phase region with the phase-separation curve. Actually, this latter characteristic is apparent and is useful in our analysis.

Daughter-phase molar volume values, deduced as described above, are shown in Fig. 12 for samples nos. 23, 24, 26, 28, and 30. More qualitative but nevertheless complementary information appears in Fig. 13, which shows the ratio of x-ray Bragg peak intensity I to I_0, the intensity at $T > T_{PS}$ plotted versus x values from Fig. 12.

To illustrate how phase diagram information can be inferred, we first use data on sample no. 23 (○). (To save space in what follows and in Tables III and IV, a 4 superscript to a structure denotes a ^{4}He-rich phase and a superscript 3 denotes a ^{3}He-rich phase.) For this highest-pressure sample, that no peak is observed for the ^{4}He-rich phase, in the region of reciprocal space used, probably means that the ^{4}He-rich phase is hcp. The ^{3}He-rich peak data show that the ^{3}He-rich phase is bcc for $x > 0.77$, because the cooling data extrapolate (by the fitted line marked 6.178 in Fig. 12) to correct pure ^{3}He molar volume at the presumed pressure of the sample (marked by the arrow and circle outside the border of Fig. 12). The discontinuities near $x \sim 0.77$ for data in both Figs. 12 and 13 probably indicate the transition from mixed hcp-bcc to solely bcc.

For each sample, similar extrapolations are shown on Fig. 12, and results are summarized in Table III. In each case is given (a) the extrapolated isotopically pure molar volume (V_e), (b) the pressure calculated from V_e using PVT data (P_e), and (c) the molar volume determined by P_m of the sample which should be compared to V_e. We estimate P_e to be the pressure on the sample during the measurements now being discussed, and we expect this to be less than P_m because of the pressure drop associated with disappearance of thermal vacancies during cooling of the sample.

TABLE III. ^{3}He-^{4}He phase-diagram information obtained from x-ray data in the phase-separated region. "From" means extrapolated from the isotopically rich phase noted and "To" means extrapolated to the isotopically pure phase noted. Volumes are per mole; the subscript e stands for an extrapolated value. See Sec. V B for definition of the superscripts and for further explanation.

Sample no.	P_m (MPa)	From	To	V (pure, P_m) (cm^3)	V_e (cm^3)	P_e (MPa)	Phase
23	6.178	^{4}He-rich	^{4}He	19.15			^{4}hcp
		^{3}He-rich	^{3}He	21.88	21.88	6.18	^{3}bcc
27	4.681	^{4}He-rich	^{4}He	19.86	20.37	3.43	^{4}bcc
		^{3}He-rich	^{3}He	22.97	24.00	3.65	^{3}bcc
26	3.565	^{4}He-rich	^{4}He	20.29	20.86	3.01	^{4}bcc
		^{4}He-rich	^{3}He	24.10	24.47	3.26	^{4}bcc-^{3}liq-^{3}bcc
28	3.475	^{4}He-rich	^{4}He	20.35	20.77	~3.0	^{4}bcc
		^{3}He-rich	^{3}He	24.20	24.45	3.28	^{3}bcc-^{3}liq
24	3.220	^{4}He-rich	^{4}He	20.51	20.66	~3.0	^{4}bcc
		^{3}He-rich	^{3}He	24.53	24.74	3.07	^{3}bcc-^{3}liq
		^{4}He-rich	^{3}He	24.53	24.72	3.08	^{4}bcc-^{3}liq-^{3}bcc
30	3.041	^{4}He-rich	^{4}He	20.63	20.98	2.83	^{4}bcc
		^{3}He-rich	^{3}He	24.78			^{3}liq

TABLE IV. Phase boundaries derived from x-ray data in the phase-separated region. Subscripts e refer to extrapolated quantities. See Sec. V B for cautionary note; the numerical values are indicative not literal.

Sample no.	Phase boundary	P_e (MPa)	x (%)	T (mK)	V_e (cm^3)
23	^{3}hcp-^{3}bcc to ^{3}bcc	6.18	77	269	21.88
27	^{4}bcc to ^{4}hcp	3.15	10	255	20.37
26	^{4}bcc-^{3}bcc-^{3}liq univariant	3.26			24.47
28	^{4}bcc-^{3}bcc to ^{4}bcc-^{3}bcc-^{3}liq	3.28	83 +	328	24.73
24	^{4}bcc-^{3}bcc to ^{4}bcc-^{3}bcc-^{3}liq	3.08	83	333	24.73
					20.63
30	^{4}bcc to ^{4}hcp	2.83	5	214	20.98

Analysis of sample no. 27 data (□) is fairly clear cut. Both the ^{4}He-rich and ^{3}He-rich phases are bcc upon cooling until the ^{4}He-rich phase transforms to hcp, as shown by decrease then disappearance its peak intensity at $x \sim 0.095$. The peak of the ^{3}He-rich phase is relatively weak since the whole sample is only 28% ^{3}He. Both the ^{4}He-rich and ^{3}He-rich phases have an extrapolated pressure of ~ 3.5 MPa, which is, within errors, about 1.1 MPa pressure change from P_m estimated[28] from the thermal vacancy concentration visible in this sample (Fig. 8).

A main result from the lower-pressure samples nos. 24 (△), 26 (○), and 28 (▽) is the determination of the ^{4}bcc-^{3}bcc-^{3}liq univariant line. This conclusion arises from two features of the data. In Fig. 12, at $x \sim 0.83$ for both samples nos. 24 (△ warming) and 28 (▽) there is a change in slope. Also, as x approaches unity, the ^{3}He-rich phase of both samples approaches a reasonable pure ^{3}He melting line value. The P_e value of sample no. 24 warming (3.07 MPa) agrees with $P_e = 3.08$ MPa obtained from the ^{4}He-rich peak of sample no. 24, which means that ^{4}bcc must be in contact with both ^{3}bcc and ^{3}liq, i.e., along a univariant. The extrapolations of ^{4}He-rich phase data of no. 26 (○) and ^{3}He-rich phase data of sample no. 28 (▽) to pure ^{3}He show the same features as sample no. 24 cooling (△). Results are shown in Table III.

The data on sample no. 30 (◇), from $0.11 > x > 0.05$, also yield interesting results. The ^{4}He-rich phase peak intensity holds about constant down to about $x = 0.06$, where it falls off, implying transition of this phase to hcp, and the ^{3}He-rich phase peak is absent, implying that this component is liquid (a result consistent with the P_e of 2.8 MPa). Alone among these samples discussed, sample no. 30 showed a large increase in peak intensity I/I_0 at phase separation (Fig. 13). Perhaps its contact with ^{3}He-rich liquid after separation allowed annealing to take place, or perhaps its passage through a mixed hcp-bcc phase above separation (Fig. 10) caused difficulties in the crystal structure. A slight increase in I/I_0 is seen in sample no. 23 (○) after it makes the mixed to pure phase transformation.

From the various results of this analysis, the pressure, isotope concentration, and molar volume of various transitions can be crudely estimated. The results of these speculations are listed in Table IV. We emphasize that the numbers in Table IV are indicative of the possibilities of this x-ray technique, but the values are not to be taken as definitive.

One firm result of our analysis is an incompatibility with the phase diagram of Tedrow and Lee,[10] who show the mixed ^{4}bcc-^{4}hcp phase meeting the phase-separation curve at a higher temperature than that at which the mixed ^{3}bcc-^{3}liq phase meets it. We, as explained above, infer coexistence of ^{4}bcc-^{3}bcc-^{3}liq, and in Fig. 14 we show a schematic phase diagram which incorporates this observation. Three other comments about the schematic diagram. (1) The width of the two phase regions as they meet the phase-separation curve is not determined. We suspect that the ^{4}bcc-^{4}hcp mixed phase width is very small, while the liquidus-solidus region near lower melting of ^{3}He-rich phase is probably wider, because the dis-

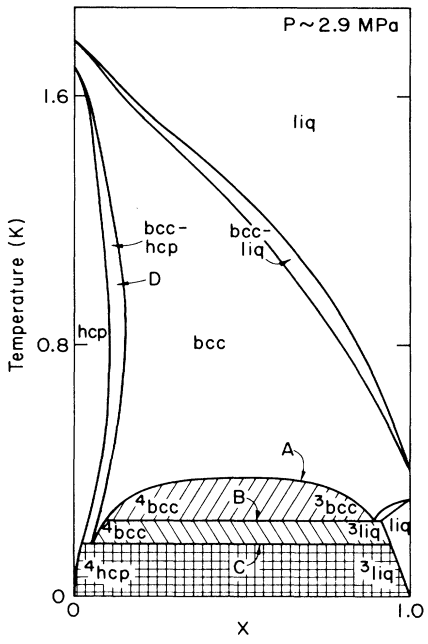

FIG. 14. Schematic T_{PS} vs x phase diagram, drawn to illustrate the qualitative differences between the conclusions in Table IV, and the phase diagram of Tedrow and Lee (Ref. 10). This diagram is not quantitative, but does show some expected features such as a very narrow region between liquidus and solidus, and reflexive behavior of the bcc-hcp mixed phase at low x. A is the phase separation curve; B the ^{4}bcc-^{3}bcc-^{3}liq univariant; C the ^{4}hcp-^{4}bcc-^{3}liq univariant. See text Sec. V B.

tortion of the V versus x picture (Fig. 12) is so much more obvious. (2) Reflexive behavior of the ^{4}bcc-^{4}hcp mixed phase boundary can explain the samples nos. 27 (Fig. 8), 29, and 30 (Fig. 10) lattice parameter data, which show anomalous changes apparently unrelated to vacancies. (3) The rather narrow width of the upper liquidus solidus is drawn simply to emphasize that the major pressure changes measured by Tedrow and Lee[10] in their 78% sample are probably due to vacancies, not to a broad liquidus-solidus region.

Other results in Table IV seem reasonable also. The mixed ^{4}hcp-^{4}bcc to ^{4}bcc transition seen at 6.1 MPa in sample no. 23 agrees qualitatively with an "interpolation" between the published T-x phase diagrams at 4.7 MPa (Ref. 9) and 11.5 MPa (Ref. 37). Also, the qualitative agreement of no. 27 conclusions with the published diagrams at 3.2 MPa (Ref. 9) and 4.5 MPa (Ref. 37) is clear.

ACKNOWLEDGMENTS

We are pleased to acknowledge the considerable assistance of R. O. Hilleke and of P. R. Granfors. This research was supported in part by the U.S. Department of Energy, Division of Materials Sciences, under Contract No. DOE-DE-AC02-76ER01198.

---

*Present address: Department of Radiation Therapy, University of Michigan Hospitals, Ann Arbor, MI 48109.

[1]H. R. Glyde, in *Rare Gas Solids,* edited by M. L. Klein and J. A. Venables (Academic, New York, 1976), Vol. I, Chap. 8.

[2]R. O. Hilleke, P. Chaddah, R. O. Simmons, D. L. Price, and S. K. Sinha, Phys. Rev. Lett. **52**, 947 (1984); R. O. Simmons, Can. J. Phys. (to be published).

[3]A. F. Andreev, in *Progress in Low Temperature Physics,* edited by D. F. Brewer (North Holland, New York, 1982), Chap. 2.

[4]M. Roger, J. H. Hetherington, and J. M. Delrieu, Rev. Mod. Phys. **55**, 1 (1983).

[5]J. H. Vignos and H. A. Fairbank, Phys. Rev. **147**, 185 (1966).

[6]D. S. Miyoshi, R. M. Cotts, A. S. Greenberg, and R. C. Richardson, Phys. Rev. A **2**, 870 (1970).

[7]V. N. Grigor'ev, B. N. Esel'son, and V. A. Mikheev, Fiz. Nizk. Temp. **1**, 5 (1975) [Sov. J. Low Temp. Phys. **1**, 1 (1975)].

[8]R. Berman and S. J. Rogers, in *Low Temperature Physics-LT9,* edited by J. G. Daunt, D. O. Edwards, F. J. Milford, and M. Yaqub (Plenum, New York, 1965), p. 262. An application of thermal conductivity measurements to study phase separation in ^{3}He-Ne and ^{4}He-Ne mixtures is reported by D. M. Livesley, J. Phys. C **16**, 2889 (1983).

[9]C. Le Pair, K. W. Taconis, R. de Bruyn Ouboter, P. Das, and E. de Jong, Physica **31**, 764 (1965).

[10]P. M. Tedrow and D. M. Lee, Phys. Rev. **181**, 399 (1960).

[11]N. E. Phillips, in *Annual Reviews in Physical Chemistry,* edited by H. Eyring (Annual Reviews, Palo Alto, California, 1968), p. 559.

[12]D. O. Edwards, A. S. McWilliams, and J. G. Daunt, Phys. Lett. **1**, 218 (1962).

[13]D. O. Edwards, A. S. McWilliams, and J. G. Daunt, Phys. Rev. Lett. **9**, 195 (1962).

[14]M. F. Panczyk, R. A. Scribner, J. R. Gonano, and E. D. Adams, Phys. Rev. Lett. **21**, 594 (1968).

[15]P. N. Henriksen, M. F. Panczyk, and E. D. Adams, Solid State Commun. **8**, 735 (1970).

[16]R. H. Arnold and P. B. Pipes, Phys. Rev. B **21**, 5156 (1980).

[17]A. S. Greenberg, W. C. Thomlinson, and R. C. Richardson, J. Low. Temp. Phys. **8**, 3 (1972).

[18]A brief preliminary account of this work is B. A. Fraass and R. O. Simmons, in Physica **107B**, 277 (1981).

[19]R. A. Swalin, *Thermodynamics of Solids* (Wiley, New York, 1972).

[20]W. J. Mullin, Phys. Rev. Lett. **20**, 254 (1968).

[21]J. H. Hetherington, W. J. Mullin, and L. Nosanow, Phys. Rev. **154**, 175 (1967).

[22]M. Uwaha, J. Phys. Soc. Jpn. **48**, 1921 (1980).

[23]J. H. Cahn, Trans. A. I. M. E. **242**, 166 (1968).

[24]J. Pipman, S. G. Lipson, J. Landau, and N. Bochner, J. Low Temp. Phys. **31**, 119 (1978).

[25]S. G. Lipson (private communication).

[26]S. M. Heald and R. O. Simmons, Rev. Sci. Instrum. **41**, 316 (1977).

[27]B. A. Fraass, P. R. Granfors, R. O. Hilleke, and R. O. Simmons, Rev. Sci. Instrum. **55**, 1455 (1984).

[28]B. A. Fraass and R. O. Simmons (unpublished).

[29]E. R. Grilly, J. Low Temp. Phys. **4**, 615 (1971); **11**, 33 (1973).

[30]S. B. Trickey, W. P. Kirk, and E. D. Adams, Rev. Mod. Phys. **44**, 668 (1982).

[31]J. Auleytner, *X-Ray Methods in the Study of Defects in Single Crystals* (Pergamon, Oxford, 1966), p. 169.

[32]P. B. Hirsch, in *Progress in Metal Physics-6,* edited by B. Chalmers and R. King (Pergamon, London, 1956), p. 282.

[33]A. E. Burgess and M. J. Crooks, Phys. Rev. **39A**, 183 (1972).

[34]R. Wanner, I. Iwasa, and S. Wales, Solid State Commun. **18**, 853 (1976); J. R. Beamish and J. P. Franck, Phys. Rev. B **28**, 1419 (1983).

[35]Since the present work was completed, S. N. Ehrlich and R. O. Simmons, J. Low Temp. Phys. (to be published) have done x-ray studies over much longer time intervals. They see hysteresis in T_{PS} of only 25 mdeg or less, and essentially regular behavior of the coexistence curve.

[36]M. Uwaha and G. A. Baym, Physica **107B**, 279 (1981).

[37]N. G. Bereznyak, I. V. Bogoyavlenskii, and B. N. Esel'son, Zh. Eksp. Teor. Fiz. **45**, 486 (1963) [Sov. Phys.—JETP **18**, 335 (1964)].